JOURNAL OF GEOPHYSICAL RESEARCH: OCEANS, VOL. 119, 509–522, doi:10.1002/2013JC009312, 2014

Importance of frictional effects and jet instability on the morphodynamics of river mouth bars and levees

Alberto Canestrelli,[1,2] William Nardin,[1,3] Douglas Edmonds,[3] Sergio Fagherazzi,[1] and Rudy Slingerland[2]

Received 29 July 2013; revised 13 November 2013; accepted 16 December 2013; published 21 January 2014.

[1] In this work, extensive numerical simulations have been performed to assess the hydrodynamic and morphodynamic behavior of a river jet debouching in a large quiescent water body. A refined three-dimensional grid has been used to capture the transition zone between a stable jet and an unstable meandering jet. The model results show that the stability number *S*, which is a function of friction and river mouth aspect ratio, and the mouth Reynolds number are the two parameters that describe the stable/unstable character of the jet. From a morphodynamic point of view, a stable jet always tends to form a mouth bar. However, a decrease of the stability number together with jet instability increase the delivery of sediments to the jet margins, favoring the formation of subaerial levees and elongated channels. Frictional effects play a major role to set the distance at which the mouth bar becomes stagnant. The importance of the stability number in setting depositional patterns at the river mouth is larger than other variables (i.e., momentum of the jet and potential vorticity) and therefore should be considered in the design of restoration schemes for deltaic land.

Citation: Canestrelli, A., W. Nardin, D. Edmonds, S. Fagherazzi, and R. Slingerland (2014), Importance of frictional effects and jet instability on the morphodynamics of river mouth bars and levees, *J. Geophys. Res. Oceans*, *119*, 509–522, doi:10.1002/2013JC009312.

1. Introduction

[2] The planform of a delta and its distributary network are set by the hydrodynamics and depositional patterns at the mouths of distributary channels. In the absence of significant waves and tides, the hydrodynamics usually consists of a bounded plane turbulent jet (Figure 1). The jet determines the sediment particle flow paths, and the evolving sediment bed influences the jet. This morphodynamic interaction then sets the number of distributaries, the rugosity of the shoreline, and ultimately the delta planform [*Edmonds and Slingerland*, 2007, 2008; *Jerolmack and Swenson*, 2007; *Edmonds et al*., 2009; *Jerolmack*, 2009; *Hoyal and Sheets*, 2009; *Martin et al*., 2009; *Chatanantavet et al*., 2012]. More recent studies have investigated the effect of wind waves [*Nardin and Fagherazzi*, 2012; *Nardin et al*., 2013] and tides [*Leonardi et al*., 2013] on jet hydrodynamics, but here we restrict our discussion to exclude them.

[3] It is unfortunate that most laboratory investigations of plane jets debouching into quiescent bodies are of the unbounded type, i.e., the experiments are performed in a way to minimize the effect of the bounding walls. Measurements are usually taken in a zone spanning from the orifice to $x/h = 1$, where x is distance along the jet axis and h is the distance between the bounding surfaces [e.g., *Bradbury* 1965; *Goldschmidt and Young*, 1975; *Everitt and Robins*, 1978; *Ramaprian and Chandrasekhara*, 1983, among others]. *Dracos et al*. [1992] pointed out at the time of his work, that few studies were performed on bounded plane jets especially for $x/h \gg 1$. *Foss and Jones* [1968] and *Holdemann and Foss* [1975], in fact, studied bounded rectangular jets, but only for $x/h < 10$. Also, these earlier studies only consider orifice geometries with aspect ratios B/h smaller than 2 where B is channel top width. These ratios are smaller than observed in typical delta distributaries. Only recently have experiments been conducted on bounded planar jets with $B/h \gg 1$ [*Rowland et al*., 2009, 2010].

[4] The turbulence characteristics of these narrow bounded jets differ from those of unbounded ones [*Dracos et al*., 1992]. Using the depth as a scaling parameter, *Draco et al*. [1992] defined three fields for a bounded jet: near ($x/h < 2$), middle ($2 < x/h < 10$), and far ($x/h > 10$). In the near field the flow is essentially the same as a classical unbounded jet, i.e., the effect of the bounding walls is not yet felt and the x-directed velocity u is uniform along the vertical axis z. In the middle field, secondary flows are present that affect the entire depth (u is nonuniform along z). For $x/h > 10$, the intensity of the turbulence is roughly constant, the jet begins to meander, and it is flanked by two set of counter-rotating vortices. The influence of the boundary is clearly seen in the turbulence spectrum of a bounded

[1]Department of Earth Sciences, Boston University, Boston, Massachusetts, USA.
[2]Department of Geosciences, Pennsylvania State University, University Park, Pennsylvania, USA.
[3]Department of Geological Sciences and Center for Geospatial Data Analysis, Indiana University, Bloomington, Indiana, USA.

Corresponding author: A. Canestrelli, Department of Geosciences, Pennsylvania State University, Deike Building, University Park, PA 16802, USA. (canestrelli@idra.unipd.it)

2169-9275/14/10.1002/2013JC009312

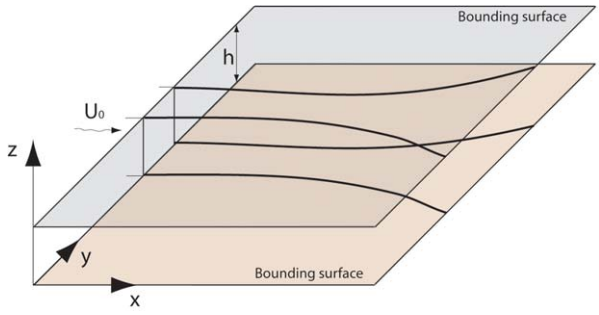

Figure 1. Sketch of a planar bounded jet.

jet. In the near field the spectrum at small wave numbers is typical of a three-dimensional cascading turbulent flow with a $-5/3$ wave number dependence [*Goldschmidt and Young*, 1975]. This is also the case of the near field in a bounded jet, but in the far field the energy transfer at small wave numbers follows a -3 wave number dependence [*Dracos et al*., 1992; *Landel et al*., 2012] typical of quasi-two-dimensional turbulence characterized by an enstrophy cascade [*Batchelor*, 1969]. This means that part of the turbulent energy is transferred from the inertial subrange to smaller wave number, i.e., to larger scale eddies. This turbulent energy transfer leads to unstable jets due to the formation of large-scale counter-rotating eddies around which the mean flow meanders.

[5] The transition from a stable, planar jet to an unstable meandering jet should be an important threshold in delta growth, because it would change the depositional patterns at the river mouth [e.g., *Rowland et al*., 2010]. Linear stability analysis is a typical theoretical approach to defining the threshold and general stability behavior of shallow jets, wakes, and mixing layers [*Jirka*, 1994; *Socolofsky and Jirka*, 2004; *Chen and Jirka*, 1997; *Jirka*, 2001; *van Prooijen and Uijttewaal*, 2002]. In this approach a parallel flow is considered, i.e., spreading of the jet is neglected. The shallow water equations are linearized, which leads to a modified Orr-Sommerfeld equation, including turbulence viscosity (ν^{T}) and bottom friction (c_f) as dissipative terms. Analyses of this type indicate jet stability has a strong dependence on friction and aspect ratio [*Jirka*, 1994]. This is embedded in the stability parameter S for shallow jets:

$$S = c_f \frac{L}{h} = \frac{c_f}{2}\frac{B}{h} \tag{1}$$

where h is the water depth, L is a jet length scale which for expanding jets we take to be equal to half mouth river width B [*Jirka*, 1994], and c_f is the friction factor in the formulation $\tau = \rho u^2 c_f/2$, with τ the bottom shear stress and u the local one-directional velocity (note that c_f can also be written as a function of the Chezy coefficient C usually adopted in shallow water simulations, i.e., $c_f = 2g/C^2$). Below a critical jet stability parameter, S_c, jet instabilities grow unimpeded; above this threshold instabilities are dampened by bottom friction. Theory and experiment suggest S_c ranges from 0.06 to 0.6 [*Uijttewaal and Booij*, 2000; *Jirka*, 2001; *vanProoijen and Uijttewaal*, 2002; *Socolofsky and Jirka*, 2004].

[6] The influence of jet instability on sedimentation patterns at a river mouth has not been fully explored, a notable exception though is the recent work by *Rowland et al*. [2010]. In this work, we are motivated by the following considerations: first, to our knowledge, no detailed numerical investigations of the transition between stable and unstable shallow jets for field-scale river mouths have been carried out. Second, most experimental investigations of shallow jets [e.g., *Rowland et al*., 2009, 2010] are limited to a single geometrical configuration. More experiments are needed with different river mouth aspect ratios, friction values, and incoming discharges to cover the entire stability parameter space. Third, the available analytical solutions for shallow jet dynamics [*Borichansky and Mikhailov*, 1966; *Wright and Coleman*, 1974; *Ozsoy*, 1977; *Ozsoy and Unluata*, 1982; *Ozsoy*, 1986; *Wang*, 1984; *Izumi et al*., 1999; *Ortega-Sánchez et al*., 2008] cannot take into account the coupled evolution of the flow field and the bottom, and can only predict the initial depositional pattern [*Ozsoy*, 1986; *Syvitski et al*., 1998]. Moreover, they cannot capture jet meandering but only predict time-averaged quantities.

[7] The aim of this paper is to define a threshold for instability (jet meandering) of a turbulent, bounded, high aspect ratio jet and to explore how frictional effects and jet instability coevolve with the patterns of sedimentation at the distributary mouth. We employ a three-dimensional model, Delft3D, that is presented in section 2. Section 3 describes the hydrodynamic results of a jet debouching into a quiescent body of water, from which a stability diagram is deduced. Section 3.2 shows the results of morphodynamic simulations and effect of instability on the depositional patterns. Discussions and conclusions are drawn in sections 4 and 5, respectively.

2. Numerical Model

[8] The numerical model chosen for our analysis is the hydrodynamic and morphodynamic Delft3D model [*Deltares*, 2013]. Here we present the main characteristics of the model together with the model setup for this work. Further details on the model can be found in *Deltares* [2013] and *Lesser et al*. [2004].

2.1. Model Description

[9] Delft3D solves the fluid flow, sediment transport, and morphological evolution in a coupled fashion. The governing equations are numerically solved in sigma-coordinates, but are here introduced in Cartesian coordinates for simplicity. Defining a coordinate system (x, y, z) with the x axis longitudinal, the y axis transversal, and the z axis vertical upward, the system of governing the three-dimensional equations for fluid flow read:

$$\left(\frac{\partial U}{\partial t} + U\frac{\partial U}{\partial x} + V\frac{\partial U}{\partial y} + W\frac{\partial U}{\partial z}\right) = -\frac{1}{\rho}\left[\frac{\partial p}{\partial x} + \frac{\partial}{\partial x}\left(2\nu_H\frac{\partial U}{\partial x}\right) + \frac{\partial}{\partial y}\nu_H\left(\frac{\partial V}{\partial x} + \frac{\partial U}{\partial y}\right) + \frac{\partial}{\partial z}\left(\nu_V\frac{\partial U}{\partial z}\right)\right] \tag{2}$$

$$\left(\frac{\partial V}{\partial t} + U\frac{\partial V}{\partial x} + V\frac{\partial V}{\partial y} + W\frac{\partial V}{\partial z}\right) = -\frac{1}{\rho}\left[\frac{\partial p}{\partial y} + \frac{\partial}{\partial x}\nu_H\left(\frac{\partial V}{\partial x} + \frac{\partial U}{\partial y}\right) + \frac{\partial}{\partial y}\left(2\nu_H\frac{\partial V}{\partial y}\right) + \frac{\partial}{\partial z}\left(\nu_V\frac{\partial V}{\partial z}\right)\right] \tag{3}$$

$$\rho g = -\frac{\partial p}{\partial z} \tag{4}$$

$$\left(\frac{\partial U}{\partial x}+\frac{\partial V}{\partial y}+\frac{\partial W}{\partial z}\right)=0 \tag{5}$$

where U, V, W are the velocities in x, y, and z directions, respectively. p is the fluid pressure, ρ is the water density, g is the gravity acceleration, v_H and v_V are the horizontal and vertical eddy viscosity, respectively.

[10] Bed load transport is computed with the formula of *van Rijn* [2007], while the suspended load transport is calculated by solving the three-dimensional diffusion-advection equation:

$$\frac{\partial c}{\partial t}+\frac{\partial Uc}{\partial x}+\frac{\partial Vc}{\partial y}+\frac{\partial (W-w_s)c}{\partial z}=\frac{\partial}{\partial x}\left(\varepsilon_{s,x}\frac{\partial c}{\partial x}\right) + \frac{\partial}{\partial y}\left(\varepsilon_{s,y}\frac{\partial c}{\partial y}\right)+\frac{\partial}{\partial z}\left(\varepsilon_{s,z}\frac{\partial c}{\partial z}\right) \tag{6}$$

where c is the suspended sediment mass concentration, w_s the hindered sediment settling velocity and $\varepsilon_{s,x}$, $\varepsilon_{s,y}$, $\varepsilon_{s,z}$ are the sediment eddy diffusivities along the three coordinate axis directions.

[11] The Reynolds stresses are modeled by using the eddy viscosity concept. For 3-D shallow water flow the stress tensor is anisotropic. The horizontal eddy viscosity coefficient, v_H, is usually much larger than the vertical eddy viscosity v_V. The vertical coefficient is computed by:

$$v_V = v_{mol} + v_{3D} \tag{7}$$

in which v_{mol} is the molecular viscosity and v_{3D} is the viscosity term modeling three dimensional turbulence. In this work, v_{3D} is computed by the three dimensional k-ε model. Note that the molecular viscosity is usually various orders of magnitude smaller than the eddy viscosity and can be neglected. The horizontal viscosity coefficient is the superposition of three terms [*Uittenbogaard et al*., 1992; *Uittenbogaard and van Vossen*, 2004]:

$$v_H = v_{mol} + v_{3D} + v_{SGS} \tag{8}$$

[12] The third term is due to subgrid scale turbulence, i.e., it is associated with the contribution of horizontal turbulent motions and forcing that are not resolved by the horizontal grid. It is modeled with the horizontal large eddy simulation technique (HLES) presented in *Uittenbogaard and van Vossen* [2004], to which the reader should refer for further details.

[13] The choice of using a numerical model that employs a large eddy simulation technique relies on the fact that direct numerical simulations are not feasible for domains with the size of tens or hundreds times the river mouth width. Moreover, it is doubtful that horizontal statistically averaging models would be able to capture large coherent structures generated by internal transverse shear instabilities [*Jirka*, 2001]. LES models appear more appropriate for this purpose [*Hinterberger et al*., 2007, 2008; *Rodi*, 2010]. Moreover, LES has been shown to correctly describe the turbulent characteristics of jets [see *Foysi et al*., 2010, among others]. As for the particular horizontal LES approach (HLES) implemented in the Delft3D model, it also appropriately describes large turbulent structures that form by shear instability [*Kernkamp and Uittenbogaard*, 2001]. Moreover, *Gerritsen et al*. [2007] showed that Delft3D succeeds in reproducing the mean streamwise velocity U, root mean square $\langle U' \rangle$, and the lateral momentum flux, as measured in the mixing layer experiment of *Uijttewaal and Booij* [2000].

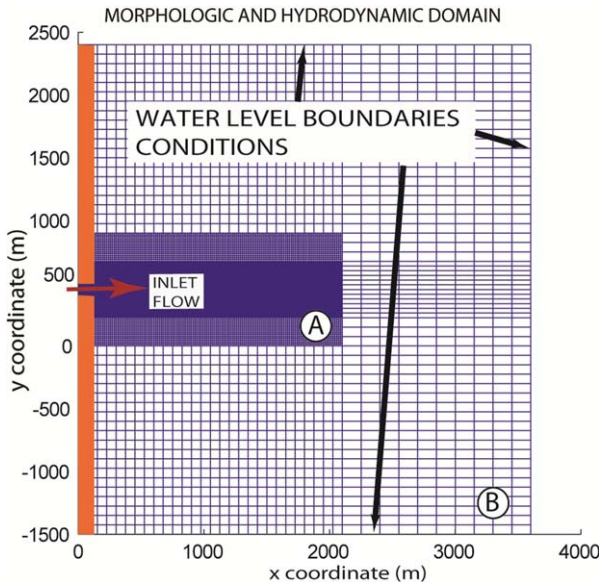

Figure 2. Computational domains and boundary conditions. The fine domain (A) is coupled with a domain (B) that is 5 times coarser in both x and y directions.

[14] In a three-dimensional LES model for shallow water problems, the mesh size should be chosen in such a way that the cutoff wave number (proportional to the inverse of the turbulent eddy length scale) lies in the inertial subrange [*van Prooijen*, 2004]. Therefore, the horizontal resolution of a LES model should at least be of the order of the water depth, so that the large-scale anisotropic turbulence is fully resolved [*van Prooijen and Uijttewaal*, 2009]. This requirement still implies long computational times, because in order to resolve vortices with the length scale of the depth, the mesh size should then be at least an order of magnitude smaller than the water depth [*van Prooijen*, 2004]. Delft3D overcomes this limitation by using a dedicated subgrid model for fine-scale 2-D motions not resolved by the coarse horizontal grid [*Kernkamp and Uittenbogaard*, 2001; *Uittenbogaard and van Vossen*, 2004]. The details of the HLES model implemented in Delft3D can be found in *Kernkamp and Uittenbogaard* [2001], *Uittenbogaard and van Vossen* [2004], and *Deltares* [2013].

2.2. Model Setup and Boundary and Initial Conditions

[15] The computational domain is rectangular and refined in the region where the jet forms (Figure 2). Moreover, we took advantage of the multidomain capability of Delft3D. In order to avoid undesirable boundary reflections and to still keep the computational time reasonably small, the fine domain was coupled with a larger domain 5 times coarser in both x and y directions. In this way, perturbations

from an oscillating jet were almost entirely dissipated by the time they reached the boundaries.

[16] Seven computational layers are used in the vertical. Note that the vertical momentum (equation (4)) employs the hydrostatic approximation, as usually done in coastal models. In our modeled jets, the horizontal length scale of the coherent structures forming in the flow field is of at least an order of magnitude larger than the vertical length scale (i.e., the water depth), and this guarantees that vertical acceleration can be neglected as compared to gravity (see Appendix A). Due to the hydrostatic approximation, the vertical velocities in our simulations are generated from continuity and not from the vertical momentum equation. Therefore, the utilization of seven vertical layers allows the presence of vertical velocities and recirculation in the coherent structure, similar to those measured by *Geyer* [1993] around headlands, thus avoiding the pitfalls of a purely 2-D solution. In fact purely 2-D solutions can overestimate the rotation rate, yielding higher vorticity and a smaller diameter of the coherent structure [e.g., *Signell and Geyer*, 1991].

[17] The initial bathymetry consists of a coastal region on the left boundary with elevation of +5 m amsl. A rectangular channel is carved into the coast with depth and width that vary among runs. The receiving basin has no slope and its depth is the same as the channel. Small amplitude ($= 0.05h$) random disturbances are added to the average depth to simulate various natural sources of perturbation. A spatially constant average depth allows us to compare model predictions with results from physical experiments that employ a horizontal bed [*Giger et al*., 1991; *Dracos et al*., 1992; *Rowland et al*. 2009, 2010]. Moreover, *Edmonds and Slingerland* [2007] found that the computed distance of the aggrading river mouth bar from the inlet is basically independent of the basin slope. The standing body of water into which the jet debouches is quiescent and devoid of waves, tides, and positive buoyancy forces (i.e., constant density).

[18] The input boundary conditions consist of a steady river discharge through the channel on the left boundary (Figure 2). In the morphodynamic simulations, a suspended concentration and bed load of a single grain size are prescribed in equilibrium with the flow. The grain size is however allowed to vary among the different simulations. At the other three boundaries a steady water elevation is prescribed (Figure 2). The thickness of the erodible sediment available at the bottom is 20 m everywhere, and the initial sediment had the same grain size of the sediment entering the domain. A spin-up time, varying among experiments, has been used before allowing any morphodynamic evolution, in order to reach fully developed hydrodynamic and sediment transport conditions.

[19] In each simulation, the time step has been varied in order to satisfy stability requirements as specified in *Deltares* [2013]. The default HLES parameters presented in *Kernkamp and Uittenbogaard* [2001] have been used. In LES models the upstream inflow boundary should contain velocity perturbations in order to represent the upstream turbulence properties in a realistic manner. We did computational experiments both prescribing and neglecting kinematic turbulent perturbations [*Van projieen and Uijttewal*, 2009], and we found no remarkable differences on the onset of instability or on the characteristics of the meandering jet and coherent structures. This is probably because the shear that establishes between the quiescent water in the basin and the high speed jet is large enough to develop hydrodynamic instability. A similar behavior was observed by *Hinterberger et al*. [2007], who noticed in a 2-D dimensional LES model that no backscatter model generating artificial random fluctuation was needed to trigger instability in a flow past a circular cylinder, while it was necessary for a mixing layer between two flows having velocities of the same order of magnitude.

[20] The morphological scale factor has been varied from a minimum of 1 to a maximum of 800, because the time scale of deposition varies with the jet velocity, the depth of the basin, and the type of sediment.

[21] The experimental design consists of about 180 numerical experiments divided into two sets: those in which the river discharge was sediment-free and the bed was fixed, and those carrying sediment over a loose boundary. In both sets the width of the channel mouth varies from 1 to 1500 m, the average channel depth from 1 mm to 30 m, the friction coefficient from 25 to 75 $m^{1/2}\ s^{-1}$, and the velocity at the mouth from 0.5 to 4 m/s. While clearly nonnatural, the small values allow comparisons to experimental results. The model jets were visually classified as meandering and therefore unstable, or time-invariant and stable.

3. Results

3.1. Hydrodynamic Stability of the Jet

[22] A jet can be destabilized either by decreasing the stability number or increasing the Reynolds number (Figure 3). The unstable jet is characterized by a meandering flow flanked by counter-rotating vortices (Figure 4). The results are similar to the laboratory experiment of *Landel et al*. [2012, Figure 8]. Note that the comparison is only qualitative since in *Landel et al*. [2012] experiment, water was flowing against gravity from the bottom to the top of the experimental apparatus, and flow was bounded by walls at both sides.

[23] *Jirka* [1994] showed that the stability of the jet should not only depend on S but also on the Reynolds number. *Chen and Jirka* [1997] found for shallow wakes that the depth-dependent Reynolds number $Re_h = Uh/\nu^T = 10^3$ is the limit above which viscous effects can be neglected. *Socolofsky and Jirka* [2004] claim that above that limit the development of the large-scale instabilities does not depend on the Reynolds number. In *Jirka* [1994] and *Socolofsky and Jirka* [2004] analysis results are shown as a width-dependent Reynolds number $Re'_B = UB/\nu^T$, that is spatially constant since the flow is approximated as parallel. While this is probably the best choice in the stability analysis problem, Re'_B is not a useful governing parameter from an engineering point of view, because in real geophysical flows U, B, and ν^T all vary along the jet and the eddy viscosity also depends on the closure model employed. Therefore, following *Dracos et al*. [1992], we here define a "river mouth" Reynolds number (Re_B) using the molecular viscosity ν, the width of the channel B, and the cross section-averaged velocity U_0 at the mouth:

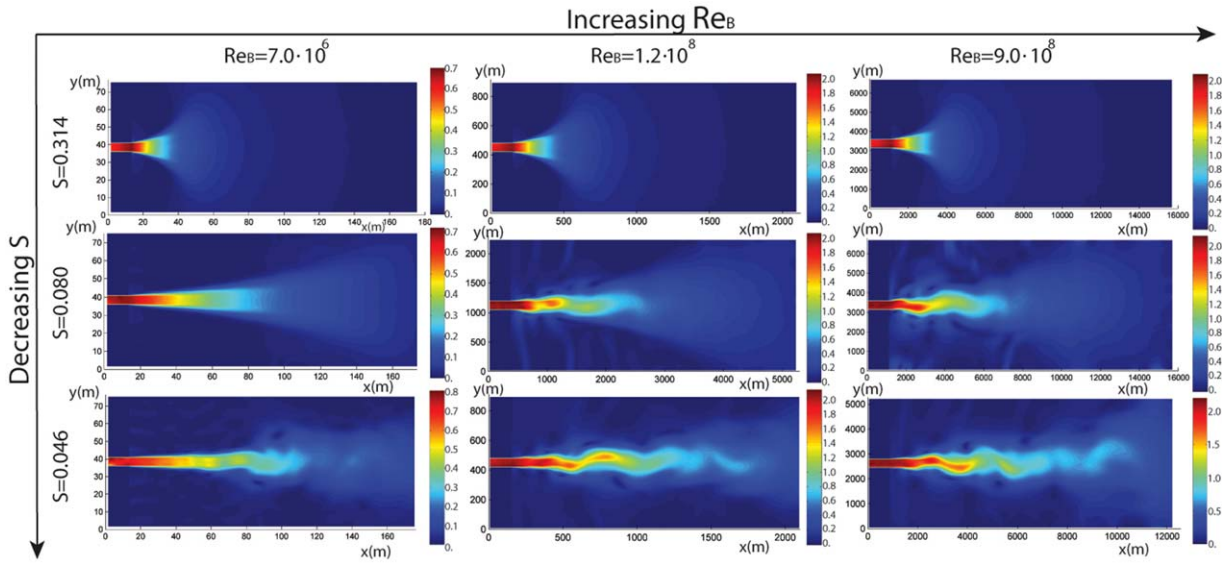

Figure 3. Transition from a stable turbulent jet to an unstable turbulent. The jet can be destabilized either by decreasing the stability number S (equation (1)) or by increasing the Reynolds number Re_B (equation (9)).

$$Re_B = \frac{U_0 B}{\nu} \tag{9}$$

[24] The critical stability number S_c has not yet been determined over ranges of Re_B values that are realistic for both laboratory scale and river mouths at the field scale. Here we conduct a series of experiments and the simulated turbulent jets representing different combinations of S and Re_B are visually classified as either unstable or stable (Figure 5). We determine a linear separation line between the two groups by mean of a linear discriminant analysis (LDA). The Fisher's linear discriminant, widely used as a linear classifier for pattern recognition [*McLachlan*, 2004] is applied to all the data providing the following relationship in the log-log space:

$$\log(S_c) = -2.87 + 0.235\ \log(Re_B) \tag{10}$$

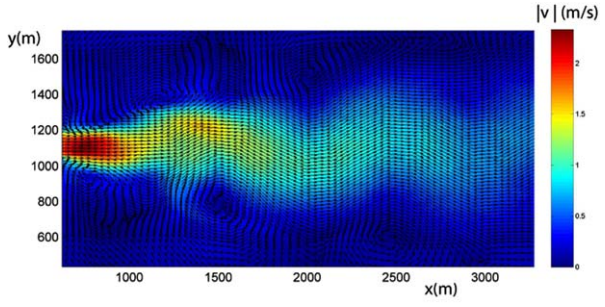

Figure 4. Example of unstable jet for a river mouth 150 m wide and a basin 6 m deep ($C = 65\ m^{1/2}\ s^{-1}$; U = 2 m/s). Colors indicate the magnitude of the velocity while arrows indicate the direction of the velocity vector. The unstable jet is characterized by a main meandering flow flanked by counter-rotating vortices.

[25] This separation line is the continuous black lines drawn in Figure 5. In the linear space, the separation line reads:

$$S_c = 1.3 \cdot 10^{-3} Re_B^{0.235} \tag{11}$$

[26] In order to assess the quality of the classification, we compute the Matthews correlation coefficient *MCC* [*Baldi et al.*, 2000]. $MCC = 1$ indicates a perfect prediction, $MCC = 0$ a prediction that is no better than random prediction and $MCC = -1$ indicates that there is total

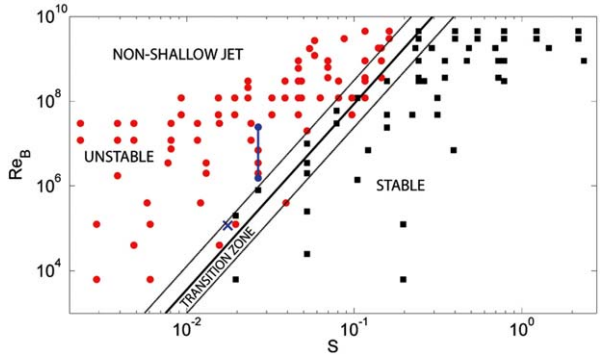

Figure 5. Stability diagram for a shallow jet ($B \geq h$) debouching in quiescent waters. The red circles indicate unstable (i.e., meandering) jets; the black squares indicate stable jets, with no large-scale horizontal coherent structures. The continuous and dotted lines represent equations (11) and (12), respectively. "x" represents the experimental data from *Rowland et al.* [2009], while the blue line ending with blue circles represents the data of the tie channels in the Fly River system (Papua New Guinea) as presented in *Day et al.* [2008] (see section 4, for a discussion).

disagreement between prediction and observation. The classification in Figure 5 provides a value of *MCC* equal to 0.84, indicating a good correlation. Moreover, we compute the maximum error as the maximum distance in the log space from a point that falls in the wrong class and the linear classifier (equation (10)) and we draw two transition lines (dashed lines in Figure 5) by horizontally shifting equation (10) by the horizontal error obtaining:

$$\begin{cases} S_c^{UP} = 0.9 \cdot 10^{-3} Re_B{}^{0.235} & (12a) \\ S_c^{DOWN} = 1.9 \cdot 10^{-3} Re_B{}^{0.235} & (12b) \end{cases}$$

[27] Equations (12) are the dotted lines in Figure 5. In this way a transition region is identified, in which both stable and unstable configurations are present, while in the stable and unstable region only simulation of the right class are present.

[28] To assess the sensitivity of the results we repeated some experiments and varied the time step, the grid resolution, and the amplitude of the random disturbances at the bottom. We found that the results of Figure 5 do not significantly depend upon the time step or the grid resolution, although some small dependence was present in the region defined as the transition zone (Figure 5), where small variations in the initial conditions can or cannot trigger instability. In the stable and unstable regions, the stability character of the jet is insensitive to time step and grid resolution.

[29] The areas of the plot not covered by data are characterized by values of Re_B and S outside the range of natural deltas and tidal inlets. In particular, the region on the upper left of the plot is characterized by B/h values equal to or lower than 1, and therefore do not belong to the category of shallow jets. Note that if instability occurs in this region, coherent structures are likely three-dimensional. However, in this work we focus on two-dimensional instability, i.e., the vertical confinement of the jet in a narrow gap changes the 3-D structure of the turbulence and a quasi-two-dimensional inverse cascade occurs that allows large eddies to grow [*Landel et al*., 2012]. In fact, in *Dracos et al*. [1992] the depth to width ratio was varied and a meandering jet was observed for $B/h = 1/16$–$1/2$, while for $B/h = 1/32$ the jet was meander-free [*Dracos et al*., 1992, Figure 5]. On the other hand, if B/h is too large (i.e., the width too large) shear instability does not occur [*Chen and Jirka*, 1998] because friction suppresses any perturbation of the straight jet.

3.2. Morphodynamics of Stable and Unstable Jets

[30] The preceding results coupled with experimental and field investigations [*Rowland*, 2007; *Rowland et al*., 2009, 2010] indicate that jet instability is present at many delta distributary mouths. Here we investigate how frictional effects and jet stability affect the morphology of mouth bars and subaqueous levees. *Edmonds and Slingerland*'s [2007] performed a series of experiments with Delft3D showing that as a channelized flow debouches into a quiescent water body, a mouth bar forms as a result of jet spreading, reduced centerline velocity, and sediment settling. The mouth bar aggrades and progrades seaward, until its height rises to about 60% of the water depth. At this point, only vertical aggradation occurs, eventually triggering a channel bifurcation [*Edmonds and Slingerland*, 2007]. Their results indicated that the distance of the bar from the river mouth, L_b, made dimensionless by the depth h, follows a power law:

$$\frac{L_b}{h} = b_1 M^{b_2} \quad (13)$$

in which $b_1 = 104$, $b_2 = 0.23$, and M is the jet momentum flux relative to area grain weight:

$$M = \frac{\rho B U^2}{(\sigma - \rho) g D_{50} B_{\max}} \quad (14)$$

where ρ_s is the density of quartz and D_{50} the median particle diameter. Equation (13) indicates that a jet carrying coarser sediment forms a bar closer to the river mouth, while an increase in momentum and depth forms a more distal bar. *Edmonds et al*. [2011] found that the value of the exponent b_2 changes for different deltas, perhaps due to the presence of other processes. When the jet is unstable, the increase of transversal eddy diffusivity due to the turbulent eddies shedding from the mouth is believed to enhance sediment deposition at the jet margins, promoting levee growth [*Rowland et al*., 2010]. *Mariotti et al*. [2013] showed by means of a dimensional analysis and two-dimensional numerical simulations that for a given mouth geometry and velocity of the jet there is an optimal diameter of sediment for which eddy diffusivity is maximum and levees' growth is favored.

[31] Based on these results, we suggest that frictional effects and jet stability also play an important role in the morphodynamics of subaqueous levees and mouth bar growth. River mouth sedimentation can be viewed as a competition between mouth bar growth and subaqueous levee growth [*Rowland et al*., 2010] because for a given sediment discharge, faster levee growth will occur at the expense of mouth bar growth (and vice versa). Jet instability increases the rate at which sediment is extracted from the jet core and delivered to the margins due to the enhanced turbulent sediment diffusion from the vortical meandering structure [*Rowland et al*., 2010]. If subaqueous levee growth dominates, then such a scenario should lead to greater distances to the mouth bar since the mouth bar sedimentation rate is lower, and fast levee growth confines the flow and forces the mouth bar to prograde basinward. Thus, for a given sediment discharge, an unstable jet should have faster levee growth and greater distances to the mouth bar.

[32] To test this idea, we start from the hydrodynamic simulations presented in section 4.1, but now add an incoming sediment load in equilibrium with the channel flow. Four different diameters have been used: 100, 200, 500, and 1000 μm. Following *Edmonds and Slingerland* [2007], we measure the distance L_b from the bar crest to the mouth when the height of the bar reaches 60% of the water depth, which is roughly when bar stagnation occurs.

[33] We decided to remove the dependence of the dimensionless momentum of the jet on B (and $B_{\max}$) and to make L_b dimensionless with B. Our model predictions indicate that the dimensionless distance to river mouth bar, L_b/B, increases in proportion to the dimensionless jet momentum

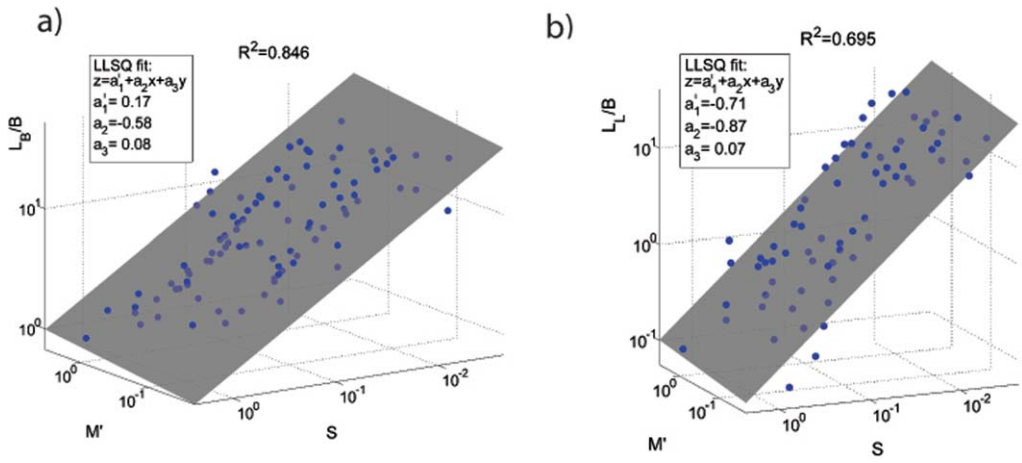

Figure 6. (a) Dimensionless distance to river mouth bar, L_b/B, increases proportionally to the dimensionless jet momentum flux M and inversely proportional to the stability factor S. The linear least squares (LLSQ) planar fit is also shown. (b) Dimensionless length L_L/B of subaerial levees shows a similar trend with S and M but the data are remarkably more scattered. Points above the fitting surface are vivid blue, while points below the surface are light blue.

flux M' and decreases in proportion to the stability factor S (Figure 6). The plot also shows a three-dimensional linear least squares (LLSQ) fit, characterized by a coefficient of determination $R^2 = 0.846$, from which the following power law is derived:

$$\frac{L_b}{B} = a_1 S^{a_2} M'^{a_3} \quad \text{with} \quad M' = \frac{\rho U^2}{(\sigma-\rho)gD_{50}} \tag{15}$$

in which $a_1 = 1.48$, $a_2 = -0.58$, and $a_3 = 0.08$. Note that in absolute value, the exponent in S, is much larger than the exponent in M. These results extend *Edmonds and Slingerland*'s [2007] contribution, and reveal that frictional effects and jet stability (as embodied in S) play even a more important role than inertial effects and cannot be neglected when predicting mouth bar distance. Note that the exponent b_2 of M in equation (13) is larger than the exponent b_2 of M' in equation (15), because we removed the dependence of the jet momentum on B.

[34] The length of the levees L_L is an indicator of the capacity of the jet to transfer sediments to its margins. We define L_L as the length of subaerial levees at the instant in which the above condition on the bar height ($= 0.6h$) is satisfied. Levees that are nonemergent at the time when flow bifurcates around the mouth bar are more likely to be dissected by the diverging currents. In Figure 6b, the dimensionless values of L_L as a function of M and S are plotted for all the simulations. The scatter of data is higher than Figure 6a, and this affects the value of R^2 of the data set. It seems that the jet momentum flux M' does not uniquely determine L_L, and for different values of M' and S the same length of emerging levee may occur. The importance of jet stability on the levee length clearly emerges in Figure 7, where we fixed the geometrical configuration and flow velocity (and thus M') and varied only S by using four different Chezy coefficients ranging from 10 to 75 $m^{1/2}$ s^{-1}. By only varying S, the morphology of the deposits undergoes a transition from a pronounced central bar with short levees that are emerging only in proximity of the mouth, to a configuration in which elongated levees emerge first and the mouth bar eventually emerges to trigger a bifurcation.

[35] Table 1 displays the length of the emerging levee, the mouth bar distance and the character of the jet (stable/unstable) for different values of the stability number. In the stable region, the length of emerging levees is zero, but by only reducing the stability number, without destabilizing the jet, the distance to the mouth bar increases. Only after the jet begins to meander the dimensionless length of the levee suddenly jumps to a large value, and then progressively increases with increasing stability number. Note that while L_L suddenly increases when the jet becomes unstable, the plot of mouth bar distance versus stability number does not display any relevant discontinuity (Figure 8).

[36] Figure 9 shows the offshore (x directed) suspended sediment transport rate Q_s in the jet with increasing distance from the mouth. The downstream decrease in suspended sediment transport indicates a loss of sediment in the y direction. Because the sediment in the centerline of the jet mainly deposits at the bar location, a decrease of longitudinal sediment transport is a measure of diffusive transport and deposition of sediments at the margins of the jet. For small values of the Chezy coefficient the slope is small, indicating that most of the sediment exiting the river mouth reaches the final location of the bar. For larger values of C, the percentage of sediment making its way to the final bar location is proportionally reduced.

[37] It has been shown in the experiments of *Rowland et al*. [2009] and in the numerical investigations of *Mariotti et al*. [2013] that an unstable jet has a larger transverse diffusivity with respect to a stable jet and this leads to a larger delivery of sediment to the jet margins. This behavior is reproduced in our numerical simulations, showing a sudden increase of the levees' length with the transition from a stable to an unstable flow field (Table 1), and a larger transversal flux of sediment with increasing S (Figure 9). However, note that in all simulations jet instability did not prevent the mouth bar from forming and becoming stagnant, but only delayed the time at which the bar formed.

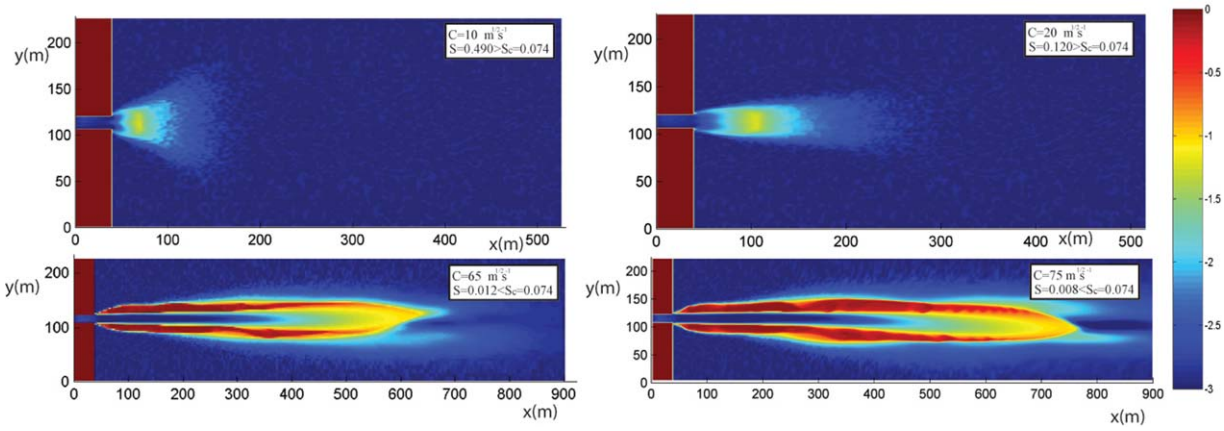

Figure 7. Morphology of the deposits for four different values of the Chezy coefficients. $Re_B = 3 \times 10^7$ and the corresponding critical value of the stability number is $S_c = 0.074$ ($B = 15$ m, $h = 3$ m, and $U = 2$ m/s).

Also in *Mariotti et al*. [2013] simulations, bars always formed, even for the simulations employing an "optimal" sediment diameter for levee formation. Note that the consequence of estimating a wrong value of the Chezy coefficient seems to affect the mouth bar distance more than considering a different d_{50}. From *Mariotti et al*. [2013, Figure 8], we can deduce that L_b/B varies only marginally, approximately from 13 to 17, when D_{50} is varied by more than one order of magnitude (from 64 to 1094 μm). From Figure 7 instead, L_b/B varies approximately from 4 to 47 when Chezy is changed from 20 to 75 $m^{1/2}$ s^{-1}. This is reflected in a higher exponent for the stability number than for the momentum flux M' (inversely proportional to d_{50}) in equation (15).

4. Discussion

4.1. Threshold for Jet Instability

[38] For a shallow mixing layer, linear stability analysis provides values of the critical stability number S_c ranging between 0.06 and 0.12 [*vanProoijen and Uijttewaal*, 2002]. For shallow jets, a value of $S_c = 0.69$ is found under inviscid ($Re \to \infty$) conditions, and it drops to about 0.5 for typical viscid conditions [*Chen and Jirka*, 1998; *Socolofsky and Jirka*, 2004]. In our fully nonlinear viscous simulations, we find lower values of S_c (Figure 5). It is difficult to directly compare these results because our stability number is defined with the width at the river mouth. The stability analysis of *Socolofsky and Jirka* [2004], instead, is based on the hypothesis of parallel streamlines (i.e., jet spreading is neglected) and therefore the critical stability number they propose should be read as a local value. However, in the case of a spreading turbulent jet, the jet width increases with distance from the inlet because of friction and lateral entrainment of water. The turbulent flow field usually takes some distance from the mouth (8–9B) to change from purely three-dimensional to quasi-two-dimensional with large horizontally oriented vortices [*Rowland et al*., 2009], and at this distance, the jet width is larger than the river width. Therefore, the effect of friction on jet stability is twofold, and it is implicitly embedded in our mouth stability number: first, a higher friction stabilizes the flow because of increased dissipation even for parallel streamlines [*Jirka*, 1994]. Second, friction increases the spreading

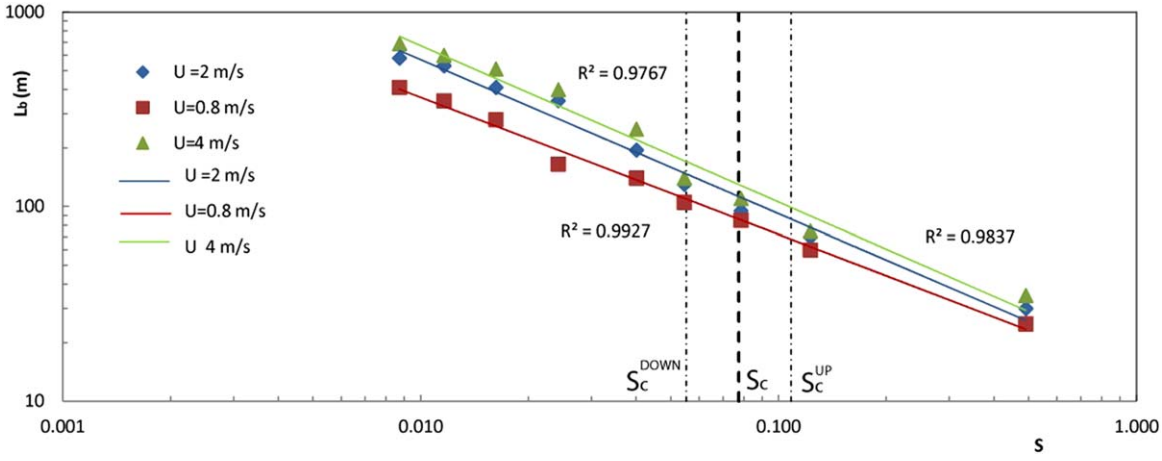

Figure 8. Plot of the mouth bar distance versus the stability number for three different velocities at the mouth (0.8, 2, and 4 m/s). d_{50} is taken equal to 0.2 mm. The colored solid lines represent the best linear regression fit. The vertical lines indicate the location of S_c, S_c^{DOWN} and S_c^{UP} from equations (11) and (12).

Table 1. Length of the Emerging Levee L_L, Mouth Bar Distance and Character of the Jet (Stable/Unstable) for Different Values of the Chezy Coefficient ($h = 3$ m, $U = 2$ m/s, and $B = 15$ m)

C	S	Stability	L_L	L_b
10	0.490	Stable	0	30
20	0.120	Stable	0	70
25	0.078	Stable	0	95
30	0.054	Stable	0	130
35	0.040	Unstable	0	195
45	0.024	Unstable	340	350
55	0.016	Unstable	460	480
65	0.012	Unstable	500	530
75	0.008	Unstable	550	580

of the jet [*Ozsoy and Unluata*, 1982; *Nardin et al*., 2013], therefore leading to higher local values of jet width and higher values of S thus further stabilizing the flow and preventing the formation of a meandering pattern.

4.2. Comparison With Natural and Experimental River Mouths

[39] To test these predictions, we plotted values from tie channels in the Fly River system [*Day et al*., 2008] and physical experiments of *Rowland* [2007, Figure 5]. Tie channels have been recently recognized as important pathways that convey sediment from the main river to the floodplains [*Day et al*., 2008; *Rowland et al*., 2009], and are usually single-thread channels. Moreover, an unstable meandering jet has been documented when water flows from the main river toward the oxbow lakes [*Rowland*, 2007; *Rowland et al*., 2009]. The tie channels surveyed by *Day et al*. [2008] have typical widths of 15–39 m and typical depths of 4.5–8.5 m. The Manning coefficient was estimated to be in the range 0.03–0.04 $m^{1/3}$ s^{-1}. Assessing a representative value of discharge is more challenging, since the discharge largely varied between channels and also in time. From *Day et al*. [2008, Figure 8], the most frequent discharges are in the range 10–180 m^3/s. Using the mean values of depth, width, and friction coefficient, a stability number $S = 0.035$ is computed. For this stability value and the mentioned range of discharges, Figure 5 indicates that the jet is unstable.

[40] As for the laboratory experiments of *Rowland et al*. [2009], a value of c_f equal to 0.004 has been estimated when the velocity data are subwindowed to exclude the influence of the jet meander [*Rowland*, 2007]. Using this value and their geometrical and boundary condition data, we compute $S = 0.013$ and $Re_B = 116{,}000$. This point falls at the upper border of the transition region (Figure 5). *Rowland* [2007] observed frictional suppression of the meandering flow when medium sand was glued to the bed of the entrance channel and when clay and plastic sediment were used to allow erosion of the bed. In the first case, the increased roughness was introduced to increase the turbulence, but it ended up increasing also the friction and overall leading to suppression of any instability. Given the sensitivity of *Rowland et al*.'s [2009] experiments to slight changes in roughness, it makes sense that their experiment plots close to the boundary between the stable and unstable region (Figure 5).

4.3. Implications for the Construction of Elongate Delta Distributary Channels

[41] Why do some deltas possess elongate distributary channels (e.g., Gilgal Abay Delta in Lake Tana, Ethiopia and the birdsfoot of the Mississippi River delta), whereas others with similar wave and tide regimes do not (e.g., Selenga River Delta in Lake Baikal, Russia)? *Kim et al*. [2009] argued that "a necessary condition for the formation of elongated or bird's-foot deltas is the existence of a prominent, well defined, prograding levee "pipeline" that aggrades to sufficient height to feed most of the sediment to the vicinity of the levee terminus." *Edmonds and Slingerland* [2010] on the other hand, argued that cohesive sediment was a sufficient condition. The numerical experiments here show a third possibility: a jet with a small stability number forms robust levees that suppress bifurcations and promote elongate distributary channels. In fact, sediment properties may not even be a necessary

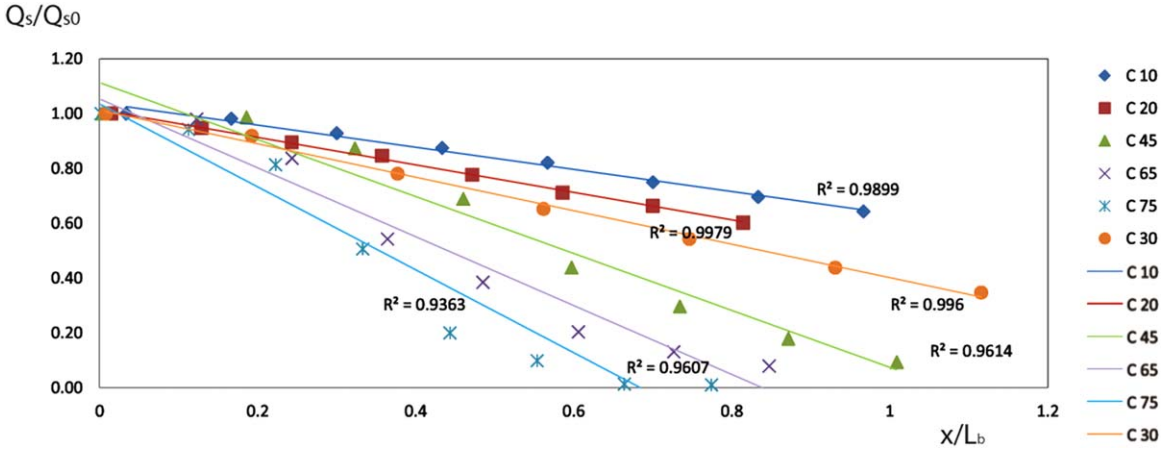

Figure 9. Plot of suspended sediment transport (Q_s) normalized by its value at the outlet (Q_{s0}) versus longitudinal distance from the mouth (x) normalized by the mouth bar distance (L_b). The solid lines represent the best linear regression fit.

condition for channel elongation; the same sediment size apparently can produce short or elongate channels (Figures 7a and 7d).

[42] Recently, *Falcini and Jerolmack* [2010] developed an elegant unifying theory based on the potential vorticity of the jet to explain why some channels are elongate and others are not. We note that the stability number also plays a role in the theory proposed by *Falcini and Jerolmack* [2010]. The latter theory states that, if the river mouth is characterized by a high value of potential vorticity, the jet will not spread laterally, thereby preserving its filament shape. On the contrary, low potential vorticity jets display rapid spreading due to friction. *Falcini and Jerolmack* [2010, equation (31)] reads:

$$\frac{d\Pi_c}{dx} = -\frac{cf}{h}\Pi_c \quad => \quad \Pi_c(x,y) = \Pi_c(0,y)\exp\left(-\frac{cf}{h}x\right) \tag{16}$$

[43] Multiplying both side for $B/2$ and using the dimensionless along axis coordinate $\xi = 2x/B$, the previous equation can be rewritten:

$$\frac{d\Pi_c}{d\xi} = -S\Pi_c => \quad \Pi_c(\xi,\zeta) = \Pi_c(0,\zeta)\exp(-S\xi) \tag{17}$$

where $\zeta = \frac{2y}{B}$. This means that the stability number represents the inverse of the dimensionless length scale of potential vorticity damping. If S is large, the potential vorticity of the jet quickly decays and bar deposition at the centerline of the jet is promoted. If S is small, potential vorticity is constant and lateral deposition (i.e., levees) is more likely to occur. Moreover, in light of the results in Figures 7–9, by decreasing S you can enter the regime where the jet is unstable and an increase of transversal diffusion leads to more pronounced levees.

[44] Scale analysis of potential vorticity carried out in *Falcini and Jerolmack* [2010] leads to the following formulation:

$$\Pi_c = \frac{Uc}{Bh} \tag{18}$$

in which c is the concentration at the river mouth. We can link the depth-averaged concentration c to the flow characteristics and sediment properties by using the (implicit) Bagnold's formulation [*van Rijn*, 2007] that reads:

$$c = K'\rho_s(1+\alpha c)\left(\frac{U^3}{ghw_s}\right) \tag{19}$$

where $\alpha = 0.00062$ and w_s is the settling velocity. For the concentrations usually found at river mouths $(1+\alpha c) \cong 1$. Therefore, neglecting as a first approximation the dependence of K' on the friction and by expressing the settling velocity by using the Stoke's law, we have that:

$$c \propto \frac{U^3}{hw_s} \rightarrow c \propto \frac{U^3}{hd_{50}^2} => \Pi_c \propto \frac{U^4}{Bh^2d_{50}^2} \tag{20}$$

[45] Note that Π_c is a dimensional quantity, and once made it dimensionless by dividing it by the constant $g^2/(h^2B)$ we have that:

$$\overline{\Pi}_c \propto \frac{U^4}{g^2d_{50}^2} \propto M'^2 \tag{21}$$

that is, the dimensionless potential vorticity $\overline{\Pi}_c$ is proportional to the square of the jet momentum. Moreover, by combining equations (17) and (21) and since B and h do not depend on ξ, we have that

$$\frac{dM'^2}{d\xi} = -SM'^2 \quad => \quad M'^2(\xi,\zeta) = M'^2(0,\zeta)\exp(-S\xi) \tag{22}$$

that can also be written as:

$$M'(\xi,\zeta) = M'(0,\zeta)\exp\left(-\frac{S}{2}\xi\right) \tag{23}$$

[46] Therefore, both M' and Π_c exhibit an exponential decay along the jet axis.

[47] Since M' is dimensionless, we suggest it may be the more appropriate parameter to use, together with S, for analyzing the morphodynamic characteristics of the jet, at least for systems in which frictional effects are not negligible. The importance of friction on the structure of the jet, in fact, was recognized by *Falcini and Jerolmack* [2010]. However, the latter claimed from equation (16) that frictional effects are small for deep outlets, implying that Π_c is a nearly conserved quantity of the system. We note that frictional effects are embedded in the dimensionless quantity S and are actually small when the aspect ratio B/h is small, since it implies a small S in equation (17), unless friction (i.e., c_f) is very large. Therefore, when S is small, Π_c also slowly decays along the jet axis, and a high value of Π_c can be safely used as an indicator for the occurrence of filament jets forming elongated channels, as successfully shown in *Falcini and Jerolmack* [2010].

[48] When frictional effects are not negligible (i.e., relatively large S), Π_c might not be a good indicator for jet behavior. To prove the latter, we show in Figure 10, four different simulations. The mouth width and the median diameter of sediments have been fixed to 15 m and 200 μm, respectively, while h and C have been varied, all simulations still being in the unstable region of Figure 5. Both Figures 10a and 10b have a depth of 3 m, but in the first case $U = 2$ m/s and $C = 45$ m$^{1/3}$ s^{-1}, while in the second case the velocity has been raised to 4 m/s and the Chezy coefficient lowered to 30 m$^{1/3}$ s^{-1}. Note that the potential vorticity Π_c in Figure 10b, computed from equation (18), is about 6 times larger than in Figure 10a. This notwithstanding, the distance of the mouth bar is more than double in Figure 10b, and the levees are well pronounced. Figure 10c has the same parameters as in Figure 10a except that the depth has been halved. Again, the potential vorticity is larger but the bar forms much closer to the mouth. Finally, Figure 10d has the same parameters as in Figures 10a and 10c, except for a depth of 4 m. The larger depth compared to Figure 10a implies a decrease of Π_c but also a decrease of S. The latter prevails, since the jet spreads less and it creates a more elongated channel.

[49] It appears that the case with larger potential vorticity does not have more pronounced levees and larger mouth bar distance (Figure 10). The same consideration holds for

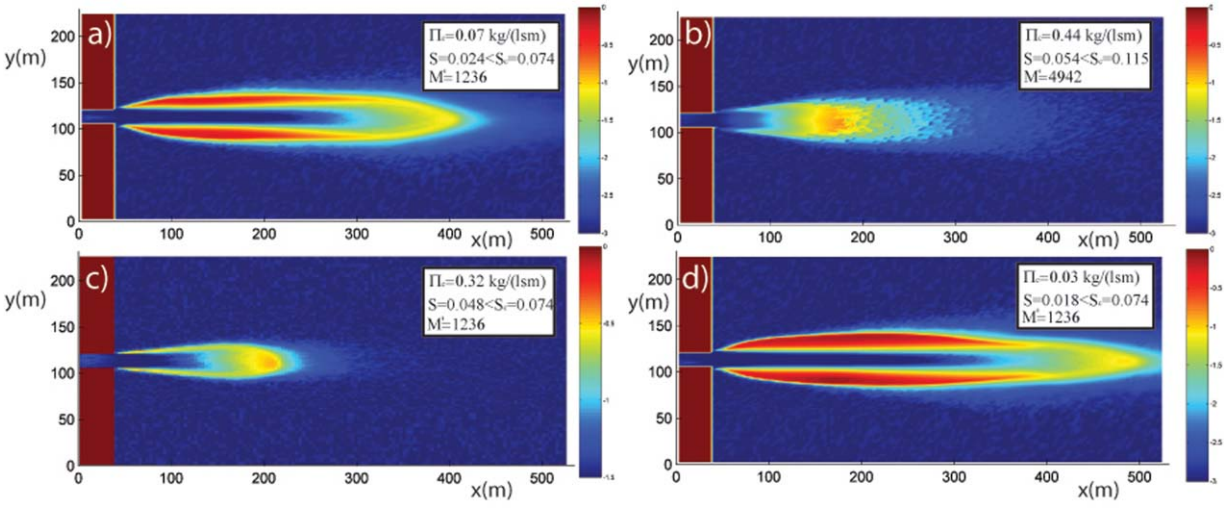

Figure 10. Variation of morphology with different values of potential vorticity, jet momentum and stability number. (a) U=2 m/s, $C = 45$ m$^{1/3}$ s^{-1}, $h = 3$ m. (b) $U = 4$ m/s, $C = 30$ m$^{1/3}$ s^{-1}, $h = 3$ m. (c) $U = 2$ m/s, $C = 45$ m$^{1/3}$ s^{-1}, $h = 1.5$ m. (d) $U = 2$ m/s, $C = 45$ m$^{1/3}$ s^{-1}, $h = 4$ m. In all the simulations, we use $d_{50} = 200$ μm.

the jet momentum. We suggest that the nonunique mapping between potential vorticity /jet momentum and depositional pattern is due to the fact that S plays a major role on setting the location of the bar. We also observe that an unstable jet does not always imply long levees, and Figure 10 shows that the smaller the value of S the larger is the jet spreading and the less pronounced are the levees, consistent with Figure 8 and equation (15).

[50] We note here that friction, expressed by the stability number S, also affects jet spreading for both stable and unstable jets. The flow field in a shallow jet can be divided in two zones: the zone of flow establishment (ZOFE), in the vicinity of the outlet, where the centerline velocity can be assumed constant, and the zone of established flow (ZOEF), showing a decay of centerline velocity [*Ozsoy and Unluata*, 1982]. When bed friction is present, the extension of the ZOFE is reduced, and to a first approximation the main characteristics of the jet can be inferred considering the ZOEF only [*Ozsoy*, 1977]. Note that in the theory of *Ozsoy* [1977] both the average jet velocity and jet width display, respectively, an exponential decay and growth along the longitudinal coordinate that depends on the stability number S. Jet spreading implies a decrease of transport capacity of the current, and lead to bar deposition [*Edmonds and Slingerland*, 2007]. The larger the spreading, the closer to the mouth the bar forms. In *Edmonds and Slingerland*'s [2007] analysis, variations of frictional effects, represented by the term S, were not included, but we have shown in section 3.2 that friction plays a role on mouth bar formation even more important than the one played by the dimensionless jet momentum.

[51] Note that in our numerical investigation, we were not able to form a channel that elongates indefinitely into the receiving basin. A bar always formed at the end of the channel. However our results, indicating a strong correlation between distance of the bar and stability number, give an indication of the likelihood (or tendency) of the jet to form single channels or channels that are likely to bifurcate.

4.4. Applications to Delta Restoration

[52] Deltaic coastlines are rapidly disappearing under the combined effect of anthropogenic sediment retention and relative sea level rise. A substantial challenge is to develop theories and practical options for restoring these environments [e.g., *Edmonds*, 2012]. Currently, a restoration option for countering land-loss in deltas include artificial diversions that deliver sediment to build deltaic land in eroding areas [*Kim et al*., 2009a; *Paola et al*., 2011]. As noted in *Falcini and Jerolmack* [2010], the initial geometry of the breach as well as the initial hydrodynamic conditions should play an important role in maximizing land growth. The results of this study indicate that, rather than using a dimensional quantity such as Π_c, the dimensionless quantities S and M' should be used to design newly created deltaic land. The designed levee breach should maximize the value of S, while keeping M' low enough to prevent the formation of an elongated channel. M' should be low but still significantly above the threshold of incipient transport, in order to speed up the process of land building. Maximizing S will depend mainly on setting the breach width because the friction coefficient is set by the grain size of the delivered sediment and the type of bed forms, and the depth h of the bay is fixed. Furthermore, the stability of bifurcation should be maintained, which requires a specific combination of c_f, M' (related to the shield stress θ through c_f) and B of the trunk stream [*Edmonds and Slingerland*, 2008].

4.5. Limitations of the Simplified Modeling Framework

[53] In the above analysis, we made many simplifying assumptions when modeling natural river mouths that may

also affect jet stability. We neglected the effect of waves, tides, positive buoyancy forces, and unsteady effects. As for waves, recent work [*Nardin and Fagherazzi*, 2012; *Nardin et al*., 2013] analyzed the effect of waves with a height up to 1 m on the process of mouth bar formation. The main result is that waves increases bottom friction and therefore the spreading of the jet, therefore reducing the distance at which bar forms. Only cases with a large stability parameter S were studied, and therefore only stable jets formed. With a higher wave height, waves destroy the bar and a wave dominated delta forms [*Nardin et al*., 2013]. How the wind waves can affect the stability of the jet should be subject of future research. On the one hand, waves would probably increase the stability parameter S by increasing bed friction. On the other hand, turbulence would be enhanced by wave breaking and by the oscillatory wave motion in the bottom boundary layer.

[54] The effect of tides on bar formation at river mouths has been analyzed in a recent paper by *Leonardi et al*. [2013]. In the fluvial dominated case, tides increase the average jet spreading, producing wider mouth bars, and speeding up their initial development [*Leonardi et al*., 2013]. Therefore, tidal oscillations have a dispersive effect on bar formation, similar to waves. Absence of stratification can also affect our numerical results, but for large discharges it is likely that the salt wedge would be pushed seaward and stratification would not strongly influence deposition (a discussion on this regard can be found in *Rowland et al*. [2010]). Moreover, *Edmonds and Slingerland* [2007] found in four numerical experiments that the process of bar formation in saline water was not substantially different from the same process in fresh water. More investigations are surely needed on this regard, to verify if the same results hold for the case of levees' formation. The fact that elongated single-thread channels also form in freshwater oxbow lakes [*Rowland et al*., 2009b; *Falcini and Jerolmack*, 2010], indicate that stratification might not be the main factor influencing their formation.

[55] Unsteady effects are also neglected in this work. *Ozsoy* [1977], by means of a rigorous order-of-magnitude analysis showed that unsteady effects are negligible at least in the tidal case, and a steady theory can be used to study quasi-steady jet properties. The same can be true for a river flood in which variations of freshwater discharge are relatively gradual. During a river flood, velocity increases, while water depth is maintained approximately constant at the river mouth [*Lamb et al*., 2012]. Therefore, it could happen that for lower discharges the jet is stable while during the maximum discharges, i.e., the formative events, the jet can be unstable. It is known that mouth bar predominantly forms during river floods [*Giosan et al*., 2005; *Maillet et al*., 2006] and during low discharge conditions, wind waves are likely to exert the main forcings on bar, that could lead to disruption of the bar itself. Therefore, in system in which there is a strong correlation between river flood and storms in the coastal region, wind waves could promote bar formation by enhancing jet spreading [*Nardin et al*., 2013]. However, in systems in which wind waves are reworking the bar for long periods while the river is inactive, it is possible that the bar could be dispersed.

[56] We finally note that high mud contents have been recognized to be a stabilizing mechanism of levees [*Edmonds and Slingerland*, 2010]. Moreover, it is recognized that rivers with a high cohesive load form narrower hydraulic sections, that can affect the hydrodynamics of the jet at the mouth [*Parker*, 1978; *Falcini and Jerolmack*, 2010]. This work also indicates that a high mud content could indirectly promote the formation of a levee-dominated river mouth since the bed would likely be smoother and devoid of bed forms, leading to a reduction of friction and jet spreading. This indirect effect of mud was not included in previous numerical experiments simulating mixed-load river mouths [*Edmonds and Slingerland*, 2010] and deserves further investigations.

5. Conclusions

[57] In this work, we show how the stable or unstable character of a shallow jet can be determined once the mouth stability number S and Reynolds number Re_B of the jet are known. In *Edmonds and Slingerland* [2007], it was shown how the distance of the mouth bar displays a power law increase with an increase of dimensionless momentum of the jet, but friction was not varied. In this work, we extend these results and highlight the importance of friction. In particular, we show that a frictionally dominated flow, i.e., characterized by a large stability number, rapidly spreads, causing a fast decrease in centerline velocity. This deceleration forms a prominent mouth bars, giving rise to short and rapidly diverging levees. On the contrary, pronounced levees and therefore elongated channels form for low stability numbers. Finally, sediment properties may not even be a necessary condition for channel elongation, because the same sediment size can produce short or elongate channels by only varying the stability number.

Appendix A

[58] In the following, a scale analysis is performed to show the validity of the hydrostatic assumption for our numerical experiments. The vertical momentum equation reads:

$$\frac{\mathrm{DW}}{\mathrm{Dt}} + \frac{1}{\rho}\frac{\mathrm{dp}}{\mathrm{dz}} = \mathrm{g} \tag{A1}$$

where D/Dt is the total time derivative (the meaning of the variables is defined in section 2.1). The hydrostatic approximation is valid whenever the condition:

$$\frac{DW}{Dt} \ll g \tag{A2}$$

is satisfied. If we indicate with L the horizontal scale of the coherent structures and with h the vertical scale (coincident with the depth), a maximum value of the vertical velocity can be estimated by continuity and reads:

$$W = \frac{Uh}{L} \tag{A3}$$

[59] The time scale of a particle of fluid moving through the system is of order L/U. Therefore condition (A2) reads:

$$R = \frac{U^2 h}{L^2 g} \ll 1 \qquad \text{(A4)}$$

[60] We use a conservative value of B as a horizontal scale of the vortex, since in our simulations $L = (4 \div 10)\ B$, see also Figure 2. It turns out that for all the simulations at the field scale, this condition is largely verified, with the maximum value of the ratio R being about 0.03. Most of the simulations at the laboratory scale had $R < 0.2$. Only for four simulations at laboratory scale, performed with a high velocity, the ratio was between 0.1 and 1. Therefore, the hydrostatic simulation is likely a good approximation and the vertical velocities obtained by continuity should not differ much from the one that would be computed by a fully nonhydrostatic model.

[61] **Acknowledgments.** Sergio Fagherazzi was supported by NSF award OCE-0948213. Alberto Canestrelli was supported first by NSF award OCE-0948213 and then by FESD/EAR-1135427. Douglas Edmonds, Rudy Slingerland, and William Nardin were supported by NSF awards OCE 1061380 and FESD/EAR-1135427. The authors also thank the anonymous reviewers and Rob Uittenbogaard at Deltares for providing the Fortran subroutines implementing the kinematic turbulent perturbations.

References

Baldi, P., S. Brunak, Y. Chauvin, C. A. F. Andersen, and H. Nielsen (2000), Assessing the accuracy of prediction algorithms for classification: An overview, *Bioinformatics*, *16*, 412–424.

Batchelor, G. K. (1969), Computation of the energy spectrum in homogeneous two-dimensional turbulence, *Phys. Fluids*, *12*, 233–239.

Borichansky, L. S., and V. N. Mikhailov (1966), Interaction of river and sea water in the absence of tides, in *Scientific Problems of the Humid Tropical Zone Deltas and Their Implications*, pp. 175–180, United Nations Educational, Scientific and Cultural Organization (UNESCO), Dacca, Pakistan.

Bradbury, L. J. S. (1965), The structure of a self-preserving turbulent plane jet, *J. Fluid Mech.*, *23*(1), 31–64.

Chatanantavet, P., M. P. Lamb, and J. A. Nittrouer (2012), Backwater controls of avulsion location on deltas, *Geophys. Res. Lett.*, *39*, L01402, doi:10.1029/2011GL050197.

Chen, D. Y., and G. H. Jirka (1997), Absolute and convective instabilities of plane turbulent wakes in a shallow water layer, *J. Fluid Mech.*, *338*, 157–172.

Chen, D., and G. H. Jirka (1998), Linear stability analysis of turbulent mixing layers and jets in shallow water layers, *J. Hydraul. Res.*, *36*, 815–830.

Day, G., W. E. Dietrich, J. C. Rowland, and A. Marshall (2008), Depositional web on the floodplain of the Fly River, Papua New Guinea, *J. Geophys. Res.*, *113*, F01S02, doi:10.1029/2006JF000622.

Deltares (2013), *Delft3D-FLOW: Simulation of Multi-Dimensional Hydrodynamic Flows and Transport Phenomena, Including Sediments—User Manual*, 614 pp., Deltares, Delft, Netherlands.

Dracos, T., M. Giger, and G. H. Jirka (1992), Plane turbulent jets in a bounded fluid layer, *J. Fluid Mech.*, *241*, 587–614.

Edmonds, D. A. (2012), Restoration sedimentology, *Nat. Geosci.*, *5*(11), 758–759.

Edmonds, D. A., and R. L. Slingerland (2007), Mechanics of middleground bar formation: Implications for the morphodynamics of delta distributary networks, *J. Geophys. Res.*, *112*, F02034, doi:10.1029/2006JF000574.

Edmonds, D. A., and R. L. Slingerland (2008), Stability of delta distributary networks and their bifurcations, *Water Resour. Res.*, *44*, W09426, doi:10.1029/2008WR006992.

Edmonds, D. A., and R. L. Slingerland (2010), Significant effect of sediment cohesion on delta morphology, *Nat. Geosci.*, *3*, 105–109.

Edmonds, D. A., D. C. J. D. Hoyal, B. A. Sheets, and R. L. Slingerland (2009), Predicting delta avulsions: Implications for coastal wetland restoration, *Geology*, *37*, 759–762, doi:10.1130/G25743A.1.

Edmonds, D. A., C. Paola, D. C. J. D. Hoyal, and B. A. Sheets (2011), Quantitative metrics that describe river deltas and their channel networks, *J. Geophys. Res.*, *116*, F04022, doi:10.1029/2010JF001955.

Everitt, K. W., and G. Robins (1978), The development and structure of turbulent plane jets, *J. Fluid Mech.*, *88*, 563–583.

Falcini, F., and D. J. Jerolmack (2010), A potential vorticity theory for the formation of elongate channels in river deltas and lakes, *J. Geophys. Res.*, *115*, F04038, doi:10.1029/2010JF001802.

Foss, J. F., and J. B. Jones (1968), Secondary flow effects in a bounded rectangular jet, *J. Basic Eng.*, *90*(2), 241–248.

Foysi, H., J. P. Mellado, and S. Sarkar (2010), Simulation and comparison of variable density round and plane jets, *Int. J. Heat Fluid Flow*, *31*, 307–314.

Gerritsen, H., E. D. De Goede, F. W. Platzek, M. Genseberger, J. A. Th. M. Van Kester, and R. E. Uittenbogaard (2007), Validation document Delft3DFLOW—A software system for 3D simulations, *WL|Delft Hydraulics Rep. X0356*. WL|Delft Hydraulics report X0356 (http://www.vliz.be/imisdocs/publications/226315.pdf).

Geyer, W. R. (1993), Three-dimensional tidal flow around headlands, *J. Geophys. Res.*, *98*(C1), 955–966.

Giger, M., T. Dracos, and G. H. Jirka (1991), Entrainment and mixing in plane turbulent jets in shallow-water, *J. Hydraul. Res.*, *29*(5), 615–642.

Giosan, L., J. Donnelly, E. Vespremeanu, J. P. Bhattacharya, C. Olariu, and F. Buonaiuto (2005), River delta morphodynamics: Examples from the Danube delta, in *River Deltas-Concepts, Models, and Examples*, edited by L. Giosan and J. Bhattacharya, pp. 393–411, SEPM (Soc. for Sediment. Geol.), Tulsa, Okla.

Goldschmidt, V. W., and M. F. Young (1975), Energy spectrum and turbulent scales in a plane air jet, Proceedings of 4th Biennial Symposium on Turbulence in Liquids, Rolla-Missouri. p. 39.

Hinterberger, C., J. Fröhlich, and W. Rodi (2007), Three dimensional and depth-averaged Large-Eddy Simulations of some shallow water flows, *J. Hydraul. Eng.*, *133*, 857–872.

Hinterberger, C., J. Fröhlich, and W. Rodi (2008), 2D and 3D turbulent fluctuations in open channel flow with $Re\tau = 590$ studied by Large Eddy Simulations, *Flow Turbul. Combust.*, *80*, 225–253.

Holdeman, J. D., and J. F. Foss (1975), Initiation, development, and decay of secondary flow in a bounded jet, *J. Fluids Eng.*, *97*(3), 342–352.

Hoyal, D. C. J. D., and B. A. Sheets (2009), Morphodynamic evolution of experimental cohesive deltas, *J. Geophys. Res.*, *114*, F02009, doi:10.1029/2007JF000882.

Izumi, N., H. Tanaka, and M. Date (1999), Inceptive topography of fluvial dominated river mouth bars, in *Proceedings of the Seventh International Symposium on River Sedimentation*, edited by A. W. Jayawardena, J. H. W. Lee, and Z. Y. Wang, A. A. Balkema, Brookfield, Vermont, 899–904.

Jerolmack, D. J. (2009), Conceptual framework for assessing the response of delta channel networks to Holocene sea level rise, *Quat. Sci. Rev.*, *28*(17–18), 1786–1800.

Jerolmack, D. J., and J. Swenson (2007), Scaling relationships and evolution of distributary networks on wave-influenced deltas, *Geophys. Res. Lett.*, *34*, L23402, doi:10.1029/2007GL031823.

Jirka, G. H. (1994), Shallow jets, in *Recent Research Advances in the Fluid Mechanics of Turbulent Jets and Plumes*, edited by P. A. Davies and M. J. Valente Neves, pp. 155–175, Kluwer Acad.

Jirka, G. H. (2001), Large scale flow structures and mixing processes in shallow flows, *J. Hydraul. Res.*, *39*(6), 567–573.

Kernkamp, H. W. J., and R. E. Uittenbogaard (2001), 2D-LES of a free surface mixing layer, in *Proceedings of the Direct and Large-Eddy Simulation Workshop 4*, edited by B. J. Geurts, R. Friedrich, and O. Metals, pp. 409–418, Enschede, Netherlands.

Kim, W., A. Dai, T. Muto, and G. Parker (2009), Delta progradation driven by an advancing sediment source: Coupled theory and experiment describing the evolution of elongated deltas, *Water Resour. Res.*, *45*, W06428, doi:10.1029/2008WR007382.

Lamb, M. P., J. A. Nittrouer, D. Mohrig and J. Shaw (2012), Backwater and river plume controls on scour upstream of river mouths: Implications for fluvio-deltaic morphodynamics, *J. Geophys. Res.*, *117*, F01002, doi:10.1029/2011JF002079.

Landel, J. R., C. P. Caulfield, and A. W. Woods (2012), Meandering due to large eddies and the statistically self-similar dynamics of quasi-two-dimensional jets, *J. Fluid Mech.*, *692*, 347–368.

Leonardi, N., A. Canestrelli, T. Sun, and S. Fagherazzi (2013), Effect of tides on mouth bar morphology and hydrodynamics, *J. Geophys. Res.*, *118*, 4169–4183, doi:10.1002/jgrc.20302.

Lesser, G., J. Roelvink, J. Van Kester, and G. Stelling (2004), Development and validation of a three-dimensional morphological model, *Coastal Eng.*, *51*, 883–915.

Maillet, G. M., C. Vella, S. Berné, P. L. Friend, C. L. Amos, T. J. Fleury, and A. Normand (2006), Morphological changes and sedimentary processes induced by the December 2003 flood event at the present mouth of the Grand Rhône River (southern France), *Mar. Geol.*, *234*, 159–177, doi:10.1016/j.margeo.2006.09.025.

Mariotti, G., F. Falcini, N. Geleynse, M. Guala, T. Sun, and S. Fagherazzi (2013), Sediment eddy diffusivity in meandering turbulent jets: Implications for depositional patterns at river mouths, *J. Geophys. Res.*, *118*, 1908–1920, doi:10.1002/jgrf.20134.

Martin, J., B. Sheets, C. Paola, and D. Hoyal (2009), Influence of steady base-level rise on channel mobility, shoreline migration, and scaling properties of a cohesive experimental delta, *J. Geophys. Res.*, *114*, F03017, doi:10.1029/2008JF001142.

McLachlan, G. J. (2004), *Discriminant Analysis and Statistical Pattern Recognition*, John Wiley, Hoboken, N. J.

Nardin, W., and S. Fagherazzi (2012), The effect of wind waves on the development of river mouth bars, *Geophys. Res. Lett.*, *39*, L12607, doi:10.1029/2012GL051788.

Nardin, W., G. Mariotti, D. A. Edmonds, R. Guercio, and S. Fagherazzi (2013), Growth of river mouth bars in sheltered bays in the presence of frontal waves, *J. Geophys. Res.*, *118*, 872–886, doi:10.1002/jgrf.20057.

Ortega-Sánchez, M., M. A. Losada, and A. Baquerizo (2008), A global model of a tidal jet including the effects of friction and bottom slope, *J. Hydraul. Res.*, *46*(1), 80–86.

Ozsoy, E. (1977), Flow and mass transport in the vicinity of tidal inlets, *Tech. Rep. TR-026*, Univ. of Florida, Coastal and Oceanogr. Eng. Lab., Gainesville, Fla.

Ozsoy, E. (1986), Ebb-tidal jets—A model of suspended sediment and mass-transport at tidal inlets, *Estuarine Coastal Shelf Sci.*, *22*(1), 45–62.

Ozsoy, E., and U. Unluata (1982), Ebb-tidal flow characteristics near inlets, *Estuarine Coastal Shelf Sci.*, *14*(3), 251–263.

Paola, C., R. Twilley, D. A. Edmonds, W. Kim, D. Mohrig, G. Parker, E. Viparelli, and V. R. Voller (2011), Natural processes in delta restoration: Application to the Mississippi Delta, *Annu. Rev. Mar. Sci.*, *3*, 3.1–3.25.

Parker, G. (1978), Self-formed straight rivers with equilibrium banks and mobile bed. Part 1: The sand-silt river, *J. Fluid Mech.*, *89*, 109–125, doi:10.1017/S0022112078002499.

Ramaprian, B. R., and D. V. Chandrasekhara (1983), *IIHR Rep. 257*, Univ. of Iowa, Iowa City, IA.

Rodi, W. (2010), Large eddy simulation of river flows, Proceedings of the International Conference on Fluvial Hydraulics, Bundesanstalt fur Wasserbau, Karlsruhe, Germany, pp. 23–32.

Rowland, J. C. (2007), Tie channels, PhD thesis, Univ. of California, Berkeley.

Rowland, J. C., M. T. Stacey, and W. E. Dietrich (2009), Turbulent characteristics of a shallow wall-bounded plane jet: Experimental implications for river mouth hydrodynamics, *J. Fluid Mech.*, *627*, 423–449, doi:10.1017/S0022112009006107.

Rowland, J. C., W. E. Dietrich, and M. T. Stacey (2010), Morphodynamics of subaqueous levee formation: Insights into river mouth morphologies arising from experiments, *J. Geophys. Res.*, *115*, F04007, doi:10.1029/2010JF001684.

Signell, R. P., and W. R. Geyer (1991), Transient eddy formation around headlands, *J. Geophys. Res.*, *96*, 2561–2575.

Socolofsky, S. A., and G. H. Jirka (2004), Large-scale flow structures and stability in shallow flows, *J. Environ. Eng. Sci.*, *3*(5), 451–462.

Syvitski, J. P., K. I. Skene, M. K. Nicholson, and M. D. Morehead (1998), Plume1.1: Deposition of sediment from a fluvial plume, *Comput. Geosci.*, *24*(2), 159–171.

Uijttewaal, W. S. J., and R. Booij (2000), Effects of shallowness on the development of free-surface mixing layers, *Phys. Fluids*, *12*(2), 392–420, doi:10.1063/1.870317.

Uittenbogaard, R. E., and B. van Vossen (2004), Subgrid-scale model for quasi-2D turbulence in shallow water, in *Shallow Flows*, edited by G. H. Jirka and W. S. J. Uijttewaal, pp. 575–582, A. A. Balkema, Leiden, Netherlands.

van Prooijen, B. C. (2004), Shallow mixing layers, PhD thesis, Delft Univ. of Technol., Delft, Netherlands.

van Prooijen, B. C., and W. S. J. Uijttewaal (2002), A linear approach for the evolution of coherent structures in shallow mixing layers, *Phys. Fluids*, *14*(12), 4105–4114, doi:10.1063/1.1514660.

van Prooijen, B. C., and W. S. J. Uijttewaal (2009), The relevance of a backscatter model for depth-averaged flow simulation, *Flow Turbul. Combust.*, *82*, 73.

van Rijn, L. C. (2007), Unified view of sediment transport by currents and waves. II: Suspended transport, *J. Hydraul. Eng.*, *133*, 668–689.

Wang, F. C. (1984), The dynamics of a river-bay-delta system, *J. Geophys. Res.*, *89*, 8054–8060.

Wright, L. D., and J. M. Coleman (1974), Mississippi river mouth processes—Effluent dynamics and morphologic development, *J. Geol.*, *82*(6), 751–778.